HHS Public Access

Author manuscript

Med Phys. Author manuscript; available in PMC 2022 May 01.

Published in final edited form as:

Med Phys. 2021 May ; 48(5): 2521–2527. doi:10.1002/mp.14786.

Gastrointestinal 4D MRI with respiratory motion correction

Adam Johansson[1,2,3], **James M. Balter**[1,4], **Yue Cao**[1,4,5]

[1]Department of Radiation Oncology, University of Michigan, Ann Arbor, Michigan, USA

[2]Department of Immunology, Genetics and Pathology, Uppsala University, Uppsala, Sweden

[3]Department of Surgical Sciences, Uppsala University, Uppsala, Sweden

[4]Department of Radiology, University of Michigan, Ann Arbor, Michigan, USA

[5]Department of Biomedical Engineering, University of Michigan, Ann Arbor, Michigan, USA

Abstract

Purpose: Gastrointestinal motion patterns such as peristalsis and segmental contractions can alter the shape and position of the stomach and intestines with respect to other irradiated organs during radiation therapy. Unfortunately, these deformations are concealed by conventional 4D-MRI techniques, which were developed to visualize respiratory motion by binning acquired data into respiratory motion states without considering the phases of GI motion. We present a method to reconstruct breathing-compensated images showing the phases of periodic gastric motion and study the effect of this motion on regional anatomical structures.

Methods: Sixty-seven DCE-MRI examinations were performed on patients undergoing MRI simulation for hepatocellular carcinoma using a golden-angle stack-of-stars sequence that collected 2000 radial spokes over 5 min. The collected data was reconstructed using a method with integrated respiratory motion correction into a time series of 3D image volumes without visible breathing motion. From this series, a gastric motion signal was extracted by temporal filtering of time–intensity curves in the stomach. Using this motion signal, breathing-corrected back-projection images were sorted according to the gastric phase and reconstructed into 21 gastric motion state images showing the phases of gastric motion.

Results: Reconstructed image volumes showed gastric motion states clearly with no visible breathing motion or related artifacts. The mean frequency of the gastric motion signal was 3 cycles/min with a standard deviation of 0.27 cycles/min.

Conclusions: Periodic gastrointestinal motion can be visualized without confounding respiratory motion using the presented GI 4D MRI technique. GI 4D MRIs may help define internal target volumes for treatment planning, aid in planning organ at risk volume definition, or support motion model development for gastrointestinal motion tracking algorithms for real time MR-guided radiation therapy.

Corresponding author: Adam Johansson, **Mailing address:** Adam Johansson, Department of Radiation Oncology, Division of Physics, University of Michigan, UH B2C490, 1500 E Medical Center Dr, Ann Arbor, MI 48109-5010, **Phone:** +1-734-936-3100, ajohanss@med.umich.edu, adam.johansson@igp.uu.se.

Conflicts of interest

The authors have no conflicts to disclose.

Keywords

4D MRI; motion correction; abdomen; deformable image registration; MRI; gastrointestinal

Introduction

Combined magnetic resonance imaging (MRI) and external beam radiation therapy ("MR Linac") systems are rapidly expanding in clinical use (1,2). These systems have already demonstrated significant advantages in efficiently gating precision radiation therapy treatments for breathing motion due to both their improved contrast over radiographic image guidance systems as well as their ability to constantly monitor the patient while treatment is being delivered. Early prototype systems have further demonstrated the ability to opportunistically take advantage of day-to-day variations in abdominal configuration to adapt abdominal radiation therapy treatments as needed based on imaging immediately prior to treatments (3–7), with promising initial results for pancreatic cancer (8–12).

While these nascent applications of configuration and (breathing) motion monitoring have already demonstrated benefit, the influence of less prominent anatomic motions, which may further limit safe delivery of tomuricidal doses, have yet to be managed effectively. The effect of gastrointestinal (GI) motion during radiotherapy has been studied using 4D CT (13) and fluoroscopy (14), with both investigations demonstrating that intrafractional gastrointestinal motion is of potentially significant magnitude to impact tumor and/or normal tissue delivered doses, and is not correlated with ventilatory motion. Aside from CT and fluoroscopy, gastrointestinal motion has also been studied using cine MRI (15–19). These investigations, while informative, fall short of full characterization of GI motions for individual patients in support of planning and/or active monitoring of treatments.

We have previously developed techniques to image dynamic changes in the abdomen free of confounding respiratory motion (20,21). In this study we present a method for four-dimensional (4D) imaging of periodic gastric motion and employ this method to study motion patterns of the stomach during MR simulation for radiation therapy.

Methods

Imaging

Under an institutional review board approved protocol, 67 MRI examinations from 32 patients (11 women; 20 men; 48–78 years old; 1–3 examinations per patient) were performed as part of a study of adaptive radiation therapy for hepatocellular carcinoma. Patients were asked not to eat anything for 2 hours before their MRI scans. A 3-T MRI scanner (Magnetom Skyra, Siemens Healthineers, Erlangen, Germany) was used with an 18-channel flexible surface coil (BodyMatrix) and 2–5 elements of the posterior coils build into the scanner table (Spine Matrix). Raw dynamic MRI data in k-space was acquired with a golden-angle stack-of-stars sequence (Radial VIBE) for 5 minutes as part of a scan protocol designed to assess liver function using DCE MRI (22–24). Sequence parameters are given in

table 1. Aside from the liver, the field of view (FOV) also covered the stomach as well as a large part of the intestines.

Respiratory motion correction

Acquired raw data was reconstructed into a time series of 3-dimensional images without visible respiratory motion using a previously described technique for DCE-MRI 4D reconstruction with respiratory motion correction (21). The technique first extracts a respiratory motion signal from the superior–inferior motion of the liver dome in an image time series reconstructed with high temporal but low spatial resolution from the stack-of-stars data. Acquired radial spokes are then sorted from exhale to inhale and reconstructed using view-sharing into a respiratory 4D MRI. A respiratory motion model is constructed by deformably aligning the breathing phases of the respiratory 4D MRI to the exhale phase and then parameterizing the resulting set of deformation vector fields by the motion signal. Finally, the breathing-compensated dynamic time series is reconstructed by deforming back-projections of individual radial spokes from the stack-of-stars sequence to the exhale state using interpolated deformation vector fields from the respiratory motion model and then combining the deformed back-projections into a time series using temporal view sharing. The temporal resolution of the view-sharing filter was 2 seconds at the center, and 58 seconds at the periphery, of k-space.

Periodic gastric motion signal

A volume of interest (VOI) encompassing the stomach was delineated manually for each examination on one of the dynamic 3D images. For each voxel in the VOI, a time–intensity curve (Figure 1) was extracted from the motion corrected image time-series. These curves exhibit oscillations due to stomach motion but also a rapid increase in intensity following contrast-agent injection. The extracted time–intensity curves were temporally filtered using a Rician filter with non-centrality parameter $\nu = 3\ \text{min}^{-1}$ and scale parameter $\sigma = 1\ \text{min}^{-1}$ to eliminate the effect on contrast agent dynamics and to emphasize gastric motion patterns which typically have a frequency of approximately $3\ \text{min}^{-1}$ (25). A total power spectrum was then formed by summing the power spectra of the individual curves (Figure 2). The mode frequency in this power spectrum was used as the non-centrality parameter for a new Rician temporal filter with scale parameter $0.25\ \text{min}^{-1}$ that was applied to the original time–intensity curves. A single curve was extracted as the first principal component (PC) of all the filtered curves as shown in Figure 3. The gastric motion signal was then determined as $\varphi = \text{atan2}(y, x)$ where x is the first PC and y its derivative. Because the gastric motion that we sought to isolate can be described as a contraction wave travelling along the stomach (26,27), φ describes the position of this wave.

Gastric 4-D MRI

To reconstruct the gastric 4D MRI, the motion-corrected back-projections of individual spokes were sorted according to their gastric cycle phase as indicated by φ. After sorting, the back-projections were combined using view sharing along the gastric dimension using a view-sharing filter (21) with a width of 200 spokes at the center and 400 spokes at the periphery of k-space.

Evaluation

The amplitude and frequency of gastric contractions was determined using the reconstructed gastric 4D MRI and the gastric motion signal. Effects of gastric motion on the stomach, liver, intrahepatic gross tumor volume (GTV) and spleen were determined using deformable image alignment of the phases of the gastric 4D MRI. This alignment was performed using open source deformable alignment software (NiftyReg) with registration parameters identical to those reported in (21).

Results

Contoured stomachs had volumes between 90 and 1100 ml with a mean of 330 ml. Gastric 4D MRIs showing periodic motion were successfully reconstructed for 61 of 67 examinations. For the remaining 6 examinations, the stomach exhibited either irregular motion patterns (4 exams), or no motion at all (2 exams). The frequency of periodic gastric motion varied among the 61 examinations from 2.5 to 3.8 min^{-1} with a mean of 3 min^{-1} and standard deviation of 0.27 min^{-1}. For the irregular motion patterns, the average mode frequency was 3 min^{-1}. Reconstructed gastric motion phase images presented with minimal motion-related artifacts, and clearly demonstrated changing configurations consistent with cyclic motions such as gastric contraction (Figure 4 and supplemental Movie S-1, S-2 and S-3).

Maximum displacements in the stomach caused by gastric motion had a mean of 5 mm and a maximum of 12 mm across examinations. Maximum displacements in the liver had a mean of 3.6 mm and a maximum of 6 mm (Figure 5) whereas the spleen had a mean displacement of 2.3 mm and a maximum of 5 mm.

Maximum displacements in the liver were significantly correlated (Pearson correlation test, $p << 0.01$) to the maximum displacement in the stomach across patients as seen in Figure 6. However, this correlation was localized to the liver periphery and was not observed ($p = 0.95$) for a subvolume defined by a 10 mm erosion of the liver VOI. No significant correlation ($p = 0.93$) of maximum stomach displacement and maximum intrahepatic GTV displacement was found for treated targets located in the liver from this patient population.

For the whole liver, spleen, and liver GTVs, maximum displacements were found at the surface of the organs (Figure 7) with smaller displacements inside the organs and larger displacements outside. For the stomach, the largest displacements occurred inside the organ with displacements of surrounding structures declining with the increasing distance to the stomach.

Stomach volumes at the first and second scan were similar for most patients (Figure 8a) as were the gastric cycle frequencies. For the few patients with large changes in stomach volume, filling did not have an obvious effect on the observed gastric cycle frequency (Figure 8b).

Because 91% of the examinations exhibited periodic gastric motion consistent with antral contraction, we conclude that this is the dominant mode of gastric motion for our

population. Other modes, such as non-periodic motion and quiescence were much less frequent (6% and 3% respectively).

Discussion

Despite large periodic gastric movements, the non-GI organs surrounding the stomach exhibit only minor movements after respiratory motion correction. With respect to periodic gastric movements, the GI tract appears almost decoupled from its surrounding. This may be a consequence of the relative stiffness of e.g. the liver to that of the stomach and intestines. Unlike the liver, GI organs close to the stomach, were observed to move in sync with the gastric cycle due to the forces exerted on them by stomach contractions.

The maximum displacements induced in surrounding structures by periodic gastric motion drop rapidly with the distance to the stomach, from a maximum of 6 mm at the stomach surface to a stationary plateau at a 20-mm distance. At this distance, the maximum displacement is dominated by the maximum registration error for all patients.

The predominantly periodic gastric motion observed in our population may have been a result of the patients not eating 2 hours prior to the MRI simulation. Therefore, patients may need to follow the same instructions prior to each radiation therapy treatment session for the GI 4D MRI to be representative. Other instructions may result in different relative frequencies of gastric motion modes with periodic motion, non-periodic motion, or quiescence.

For the few patients observed with non-periodic gastric motion, the presented GI 4D MRI technique is not applicable. To image this motion, fast dynamic 3D imaging techniques, possibly accelerated by compressed sensing or artificial intelligence, need to be developed.

The large inter-examination changes in stomach volume observed for two patients were likely caused by the patients not following the no-eating instructions before the second scan. For these patients, stomach filling did not affect the gastric cycle frequency.

The presented method requires manual delineation of a stomach VOI to extract the GI motion signal. This delineation need not be precise. It is enough for the VOI to cover the stomach with a margin. Eliminating this manual step would allow a GI 4D MRI to be reconstructed without operator intervention after scanning. For this purpose, automatic stomach segmentation driven by deep learning could be used in future studies.

This investigation provides a general framework for investigation of gastrointestinal motions in the abdomen. While the focus of the initial investigation was related to motions of the stomach and their impact on surrounding anatomic configurations, the methodology presented herein could be applied to further explore motion as well as longer-term configuration changes of the abdomen at locations distal to the stomach.

Tissue displacements due to GI motions are often smaller in amplitude than displacements caused by breathing. Determining margins for target volumes or organs at risk from the GI 4D MRI alone is not meaningful. Instead, the movements observed in the GI 4D MRI could

be modelled and composed with the previously constructed respiratory motion model (21) into a combined respiratory and gastrointestinal motion model. From this model patient specific margin or population margins could be estimated. The model could also help guide gating or tracking (28) during irradiation for MR-guided radiation therapy with MR-linacs.

Conclusions

Periodic gastrointestinal motion can be visualized without confounding respiratory motion using the presented GI 4D MRI technique. Periodic gastric motion can cause tissue displacements of up to 10 mm for other GI organs. The effect on other surrounding organs such as liver and spleen is smaller with a maximum observed displacement of 6 mm.

Supplementary Material

Refer to Web version on PubMed Central for supplementary material.

Acknowledgements

This work was supported by NIH/NCI P01 CA059827 and NIH/NIBIB R01 EB016079. The prototype Radial VIBE sequence was provided by Siemens Healthineers under a research agreement.

Data availability statement

Raw data were generated at the University of Michigan. Derived results from the data that support this study can be accessed from the corresponding author upon request.

Abbreviations:

4D MRI	four-dimensional MRI
DCE MRI	dynamic contrast-enhanced MRI
FOV	field of view
MR	magnetic resonance
VIBE	volume-interpolated breathhold examination
GI	gastrointestinal
GTV	gross tumor volume
PCA	principal component analysis
PC	principal component
VOI	volume of interest

References

1. Raaymakers BW, Kontaxis C, Bol GH, de Boer JCJ, Knox C. First Patients Treated With a 1.5T MRI-Linac: Clinical Proof of Concept of a High-Precision, High-Field MRI Guided Radiotherapy Treatment. Phys Med Biol. 2017;62(23):L41–51. [PubMed: 29135471]
2. Mutic S, Dempsey JF. The ViewRay System: Magnetic Resonance-Guided and Controlled Radiotherapy. Semin Radiat Oncol. 2014;24(3):196–9. [PubMed: 24931092]
3. Acharya S, Fischer-Valuck BW, Kashani R, Parikh P, Yang D, Zhao T, Green O, Wooten O, Li HH, Hu Y, Rodriguez V, Olsen L, Robinson C, Michalski J, Mutic S, Olsen J. Online Magnetic Resonance Image Guided Adaptive Radiation Therapy: First Clinical Applications. Int J Radiat Oncol Biol Phys. 2016;94(2):394–403. [PubMed: 26678659]
4. Henke L, Kashani R, Yang D, Zhao T, Green O, Olsen L, Rodriguez V, Wooten HO, Li HH, Hu Y, Bradley J, Robinson C, Parikh P, Michalski J, Mutic S, Olsen JR. Simulated Online Adaptive Magnetic Resonance–Guided Stereotactic Body Radiation Therapy for the Treatment of Oligometastatic Disease of the Abdomen and Central Thorax: Characterization of Potential Advantages. Int J Radiat Oncol Biol Phys. 2016;96(5):1078–86. [PubMed: 27742541]
5. Fischer-Valuck BW, Henke L, Green O, Kashani R, Acharya S, Bradley JD, et al. Two-and-a-half-year clinical experience with the world's first magnetic resonance image guided radiation therapy system. Adv Radiat Oncol. 2017;2(3):485–93. [PubMed: 29114617]
6. Henke L, Kashani R, Robinson C, Curcuru A, DeWees T, Bradley J, Green O, Michalski J, Mutic S, Parikh P, Olsen J. Phase I trial of stereotactic MR-guided online adaptive radiation therapy (SMART) for the treatment of oligometastatic or unresectable primary malignancies of the abdomen. Radiother Oncol. 2018;126(3):519–26. [PubMed: 29277446]
7. Balter JM, Brock KK, Litzenberg DW, McShan DL, Lawrence TS, Ten Haken R, McGinn CJ, Lam KL, Dawson LA. Daily targeting of intrahepatic tumors for radiotherapy. Int J Radiat Oncol Biol Phys. 2002;52(1):266–71. [PubMed: 11777645]
8. Jiang N, Cao M, Lamb JM, Sheng K, Mikaeilian A, Low D, Raldow A, Steinberg ML, Lee P. Outcomes Utilizing MRI-Guided and Real-Time Adaptive Pancreas Stereotactic Body Radiotherapy (SBRT). Int J Radiat Oncol. 2017;99(2):S146.
9. Rudra S, Jiang N, Rosenberg SA, Olsen JR, Parikh PJ, Bassetti MF, Lee P. High Dose Adaptive MRI Guided Radiation Therapy Improves Overall Survival of Inoperable Pancreatic Cancer. Int J Radiat Oncol. 2017;99(2):E184.
10. Weiner A, Chen I, Curcuru A, Henke L, Green O, Markovina S, Gay H, Robinson C, Roach M, Olsen J, Kashani R, Parikh P. (P031) Early Clinical Experience in High Dose MRI Guided Adaptive Radiation Therapy for Inoperable Pancreatic Cancer. Int J Radiat Oncol. 2017;98(2S):E23.
11. Mittauer K, Rosenberg S, Guerts M, Bassetti M, Chen I, Henke L, Olsen J, Kashani R, Wojciezynski A, Harari P, Labby Z, Hill P, Parikh P, Bayouth J. Indications for Online Adaptive Radiotherapy Based On Dosimetric Consequences of Interfractional Pancreas-To-Duodenum Motion in MRI-Guided Pancreatic Radiotherapy. Med Phys. 2018;43(6Part33):1.
12. Bohoudi O, Bruynzeel AME, Senan S, Cuijpers JP, Slotman BJ, Lagerwaard FJ, Palacios MA. Fast and robust online adaptive planning in stereotactic MR-guided adaptive radiation therapy (SMART) for pancreatic cancer. Radiother Oncol. 2017;125(3):439–44. [PubMed: 28811038]
13. Lischalk JW, Kole TP, Anjum HM, Obayomi-Davies O, Rashid A, Unger K. Four-dimensional computed tomography prediction of inter- and intrafractional upper gastrointestinal tumor motion during fractionated stereotactic body radiation therapy. Pract Radiat Oncol. 2016;6(3):176–82. [PubMed: 26746816]
14. Watanabe M, Isobe K, Takisima H, Uno T, Ueno N, Kawakami H, Shigematsu N, Yamashita M, Ito H. Intrafractional gastric motion and interfractional stomach deformity during radiation therapy. Radiother Oncol. 2008;87(3):425–31. [PubMed: 18207268]
15. Alyami J, Spiller RC, Marciani L. Magnetic resonance imaging to evaluate gastrointestinal function. Neurogastroenterol Motil. 2015;27(12):1687–92. [PubMed: 26598049]
16. de Jonge CS, Smout AJPM, Nederveen AJ, Stoker J. Evaluation of gastrointestinal motility with MRI: Advances, challenges and opportunities. Neurogastroenterol Motil. 2018;30(1):1–7.

17. Hoad CL, Menys A, Garsed K, Marciani L, Hamy V, Murray K, Costigan C, Atkinson D, Major G, Spiller RC, Taylor SA, Gowland PA. Colon wall motility: Comparison of novel quantitative semi-automatic measurements using cine MRI. Neurogastroenterol Motil. 2016;28(3):327–35. [PubMed: 26612075]
18. Menys A, Hamy V, Makanyanga J, Hoad C, Gowland P, Odille F, Taylor SA, Atkinson D. Dual registration of abdominal motion for motility assessment in free-breathing data sets acquired using dynamic MRI. Phys Med Biol. 2014;59(16):4603–19. [PubMed: 25079109]
19. Feng M, Balter JM, Normolle D, Adusumilli S, Cao Y, Chenevert TL, Ben-Josef E. Characterization of Pancreatic Tumor Motion Using Cine MRI: Surrogates for Tumor Position Should Be Used With Caution. Int J Radiat Oncol Biol Phys. 2009;74(3):884–91. [PubMed: 19395190]
20. Johansson A, Balter J, Cao Y. Rigid-body motion correction of the liver in image reconstruction for golden-angle stack-of-stars DCE MRI. Magn Reson Med. 2018;79(3):1345–53. [PubMed: 28617993]
21. Johansson A, Balter JM, Cao Y. Abdominal DCE-MRI reconstruction with deformable motion correction for liver perfusion quantification. Med Phys. 2018;45(10):4529–40. [PubMed: 30098044]
22. Wang H, Feng M, Jackson A, Ten Haken RK, Lawrence TS, Cao Y. Local and global function model of the liver. Int J Radiat Oncol Biol Phys. 2016;94(1):181–8. [PubMed: 26700712]
23. Cao Y, Wang H, Johnson TD, Pan C, Hussain H, Balter JM, Normolle D, Ben-Josef E, Ten Haken RK, Lawrence TS, Feng M. Prediction of liver function by using magnetic resonance-based portal venous perfusion imaging. Int J Radiat Oncol Biol Phys. 2013;85(1):258–63. [PubMed: 22520476]
24. Simeth J, Johansson A, Owen D, Cuneo K, Mierzwa M, Lawrence T, Feng M, Cao Y. Quantification of liver function by linearization of a 2-compartment model of gadoxetic-acid uptake using dynamic contrast enhanced magnetic resonance imaging. NMR Biomed. 2018;31(6):e3913 1–15. [PubMed: 29675932]
25. Marciani L, Young P, Wright J, Moore R, Coleman N, Gowland PA, Spiller RC. Antral motility measurements by magnetic resonance imaging. Neurogastroenterol Motil. 2001;13(5):511–8. [PubMed: 11696113]
26. Lammers WJEP, Stephen B, Slack JR. Similarities and differences in the propagation of slow waves and peristaltic waves. Am J Physiol Liver Physiol. 2002;283(3):G778–86.
27. O'Grady G, Du P, Cheng LK, Egbuji JU, Lammers WJEP, Windsor JA, Pullan AJ. Origin and propagation of human gastric slow-wave activity defined by high-resolution mapping. AJP Gastrointest Liver Physiol. 2010;299(3):G585–92.
28. Stemkens B, Tijssen RH, de Senneville BD, Lagendijk JJ, van den Berg CA. Image-driven, model-based 3D abdominal motion estimation for MR-guided radiotherapy. Phys Med Biol. 2016;61(14):5335–55. [PubMed: 27362636]

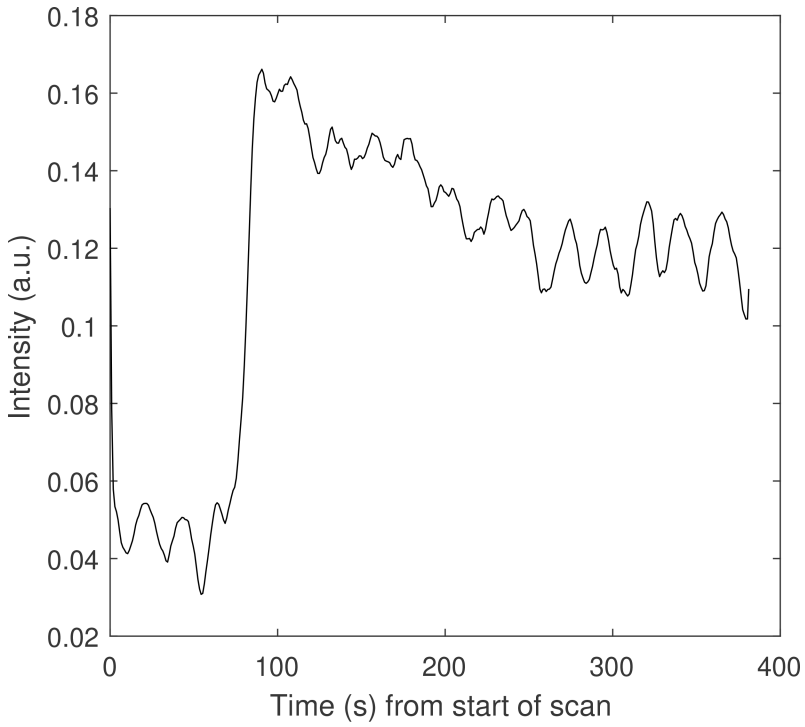

Figure 1.
Sample time–intensity curve for a single voxel inside a stomach VOI for one patient. The oscillations in the curve are due to periodic gastric motion. The large intensity increase one minute into the scan is caused by the contrast agent (Gd-BOPTA) injection.

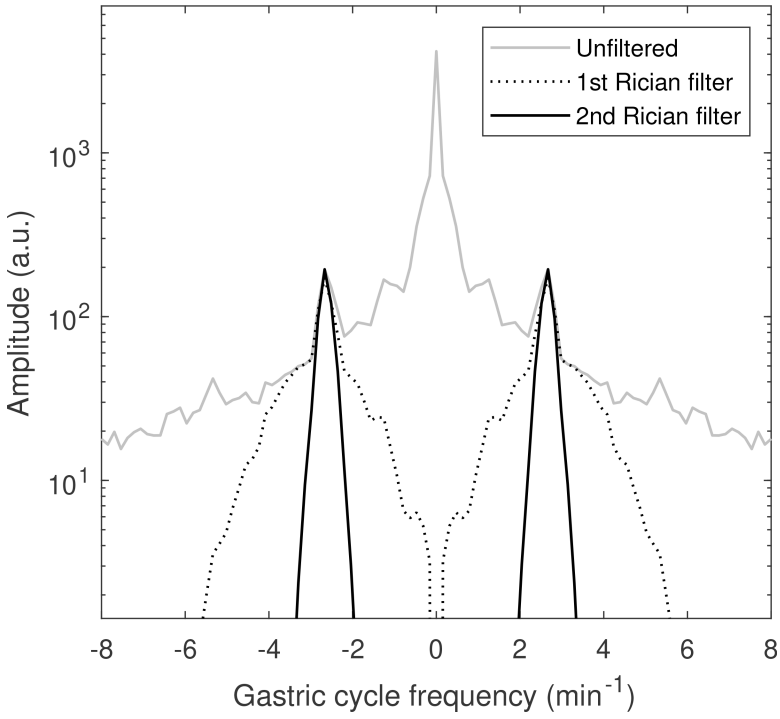

Figure 2.

Total power spectrum of gastric time-intensity curves before filtering (solid gray) and after application of the first (dotted black) and second (solid black) Rician filters. The filters select the two peaks corresponding to periodic gastric motion.

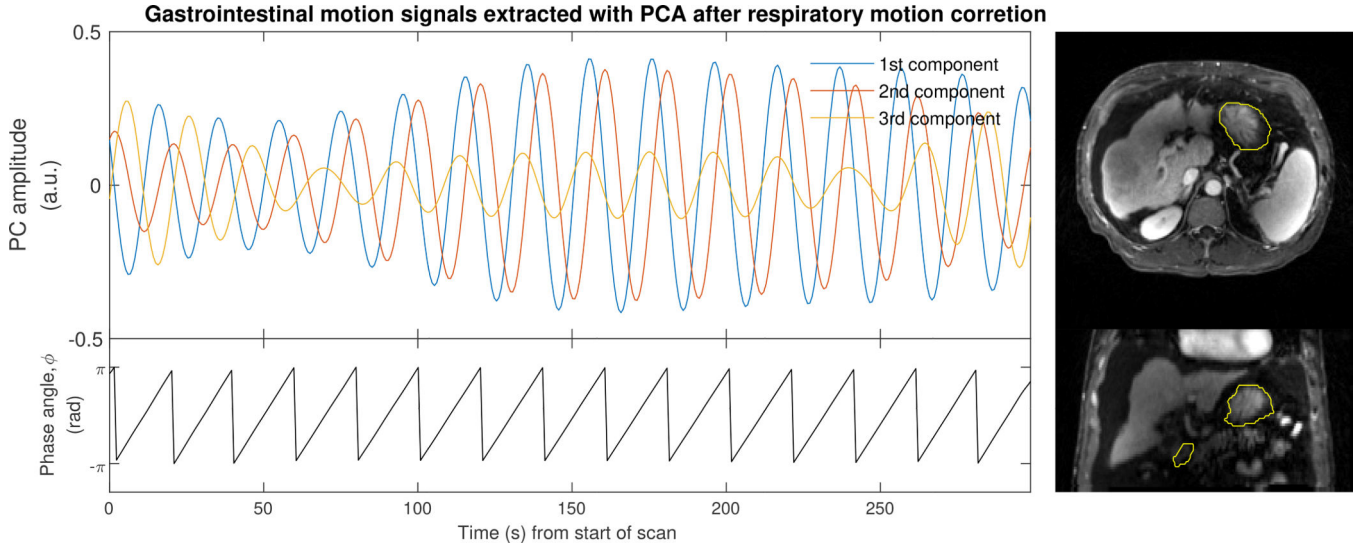

Figure 3.

The first three PCs extracted from filtered time–intensity curves within a VOI encompassing the stomach (yellow contours on right). The gastric motion signal, φ, is defined as the phase of the first PC.

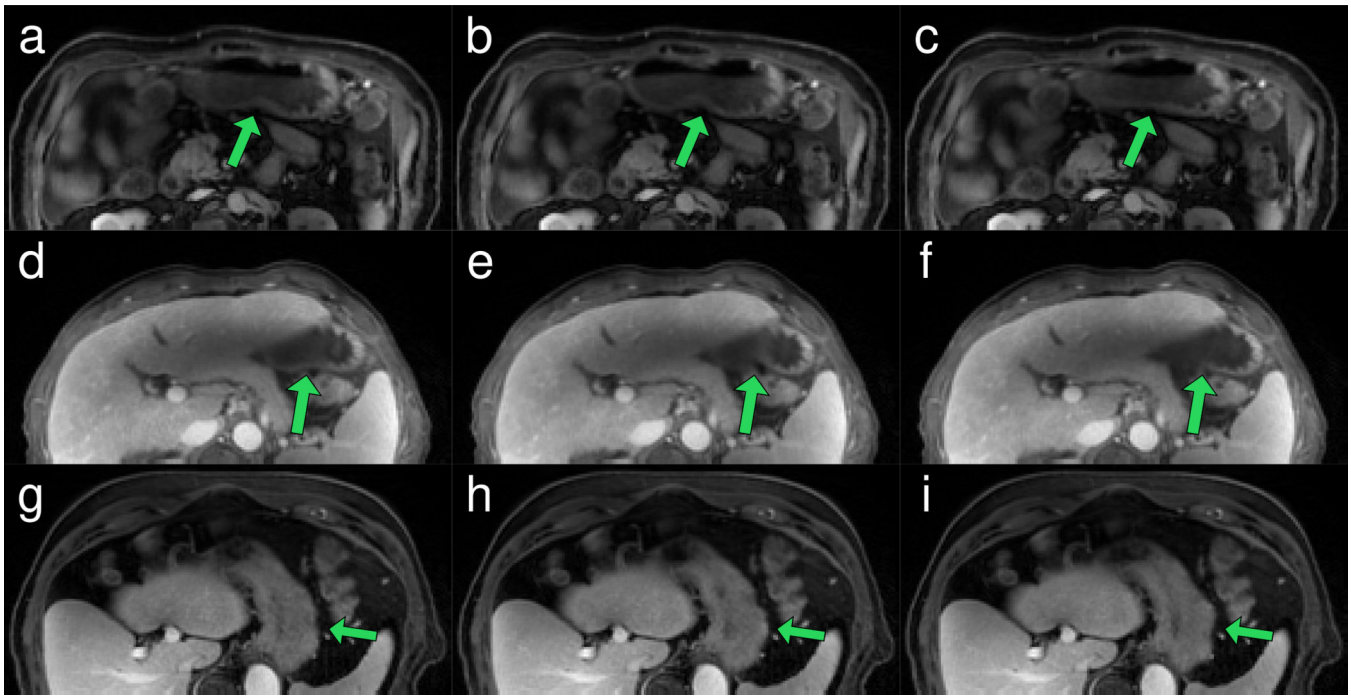

Figure 4.

Three phases of a periodic gastric motion cycle from three separate patients. Each phase is shown in planes through the lower abdomen (a, b, c) for patient 1, liver lateral tip (d, e, f) for patient 2 and inferior liver and spleen (g, h, i) for patient 3. Green arrows indicate large stomach tissue movements. Movies of the three patients are available as supplemental materials Movie S-1, S-2 and S-3.

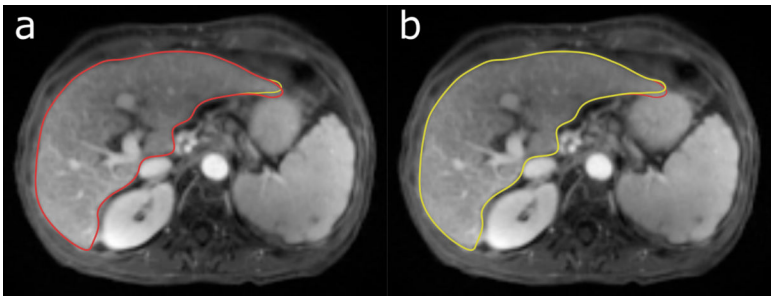

Figure 5.

The largest observed liver deformation (6 mm) caused by periodic gastric motion. Two phases are shown, half a gastric cycle apart. The red contour shows the shape of the liver in (a) and the yellow contour the shape in (b).

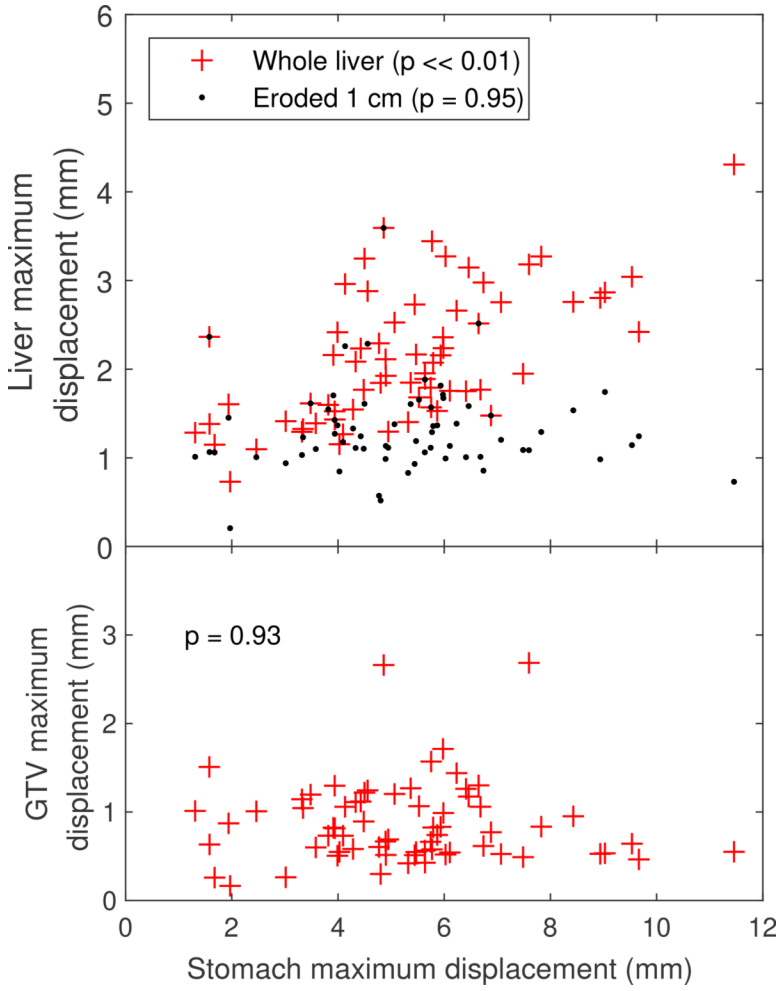

Figure 6.
Maximum displacements over the gastric cycle for the stomach versus the liver (top) and the intrahepatic GTV (bottom).

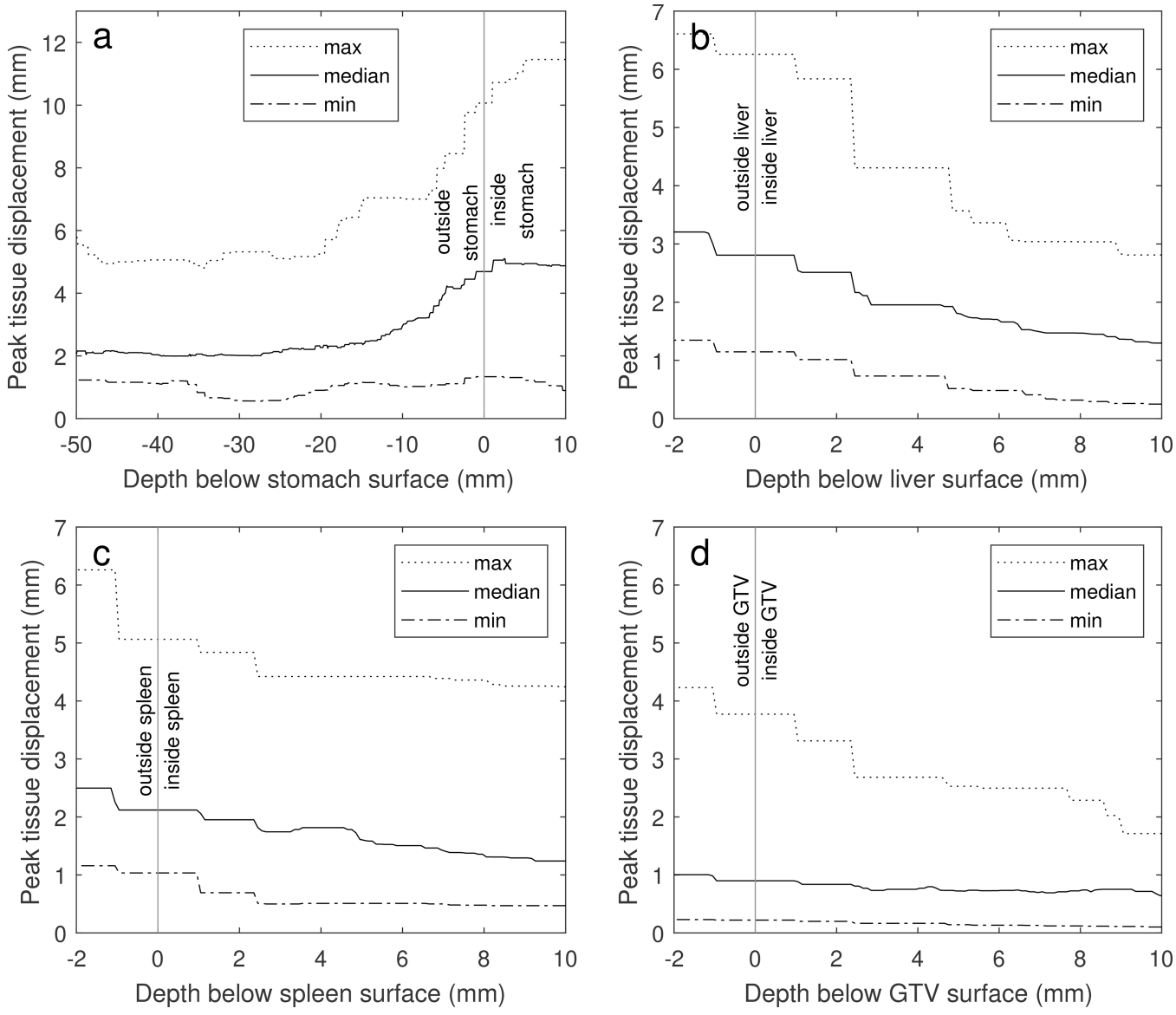

Figure 7.

Peak GI-induced displacements of locations inside the stomach (a), liver (b), spleen (c) and liver GTV (d) vs the depth of the locations below the structure surfaces. Negative depths represent locations outside the structures. The dotted, solid and dashed lines show the maximum, median and minimum peak displacements across all patients.

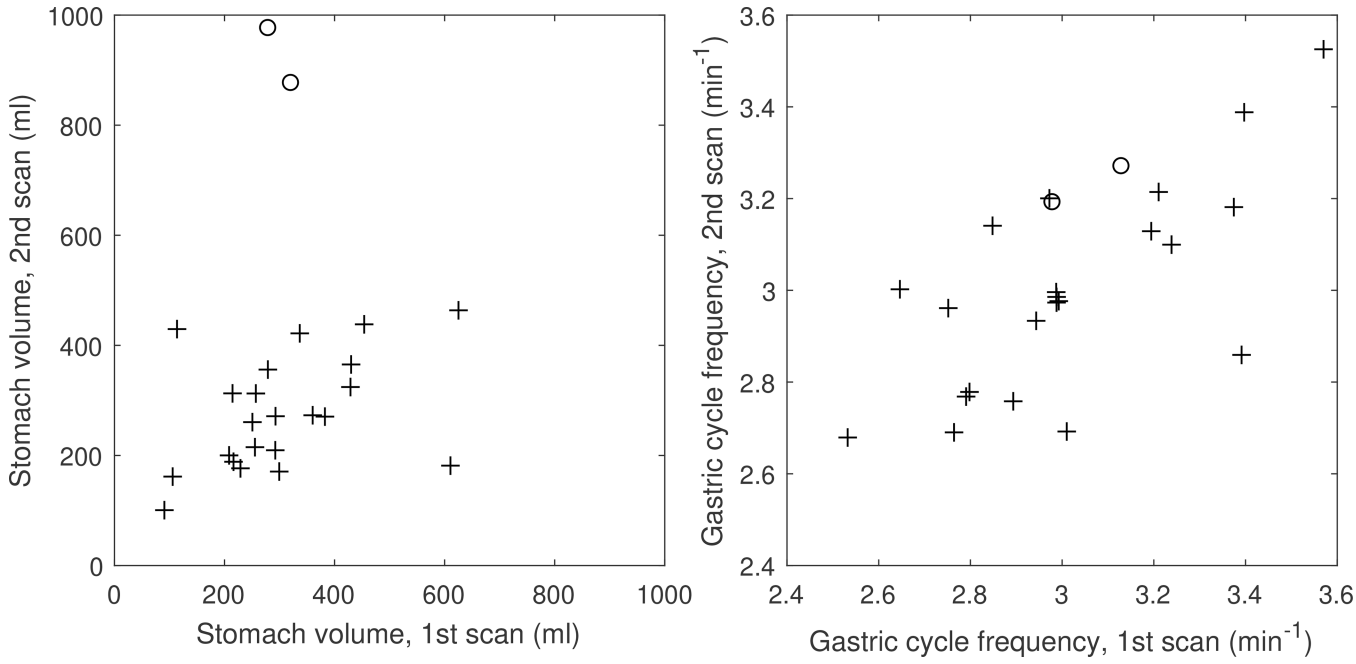

Figure 8.

Interfractional changes of stomach volume and gastric cycle frequencies. Circles indicate patients whose stomach volumes changed by more than 500 ml between scans.

Table 1.

DCE-MRI sequence parameters

Sequence parameters	
Sequence type	Golden-angle stack-of-stars spoiled gradient echo with fat suppression
Echo time	1.14–1.21 ms
Repetition time	2.72–4.51 ms
Flip angle	10°–14°
Image matrix size	192 × 192
Number of slices	64
Number of partitions	46 (acquired) + 12 (partial Fourier)
Number of radial spokes	2000
In-plane voxel size	2–2.45 mm
Slice thickness	3–4 mm